Electronic Supplementary Information (ESI)

Low-Melting, Ether-Functionalised Lithium Salts for Enhanced Ion Transport in Molten Salt Electrolytes

Yuna Matsuyama,[a] Frederik Philippi,[b] Taku Sudoh,[a] David Pugh,[c] Saki Sawayama,[d] Kenta Fujii,[d] Seiji Tsuzuki,[e] Md. Sharif Hossain*[,a,f] and Kazuhide Ueno*[,a,e]

[a] *Department of Chemistry and Life Science, Yokohama National University, 79-5 Tokiwadai, Hodogaya-ku, Yokohama, Kanagawa, 240-8501, Japan*
[b] *Laboratoire de Chimie ENS de Lyon, Campus Monod Room M6.056, 46 Allée d 'Italie, 69364 Lyon Cedex 07, France*
[c] *Department of Chemistry, King's College London, Britannia House, 7 Trinity Street, London SE1 1DB, UK*
[d] *Graduate School of Sciences and Technology for Innovation, Yamaguchi University, 2-16-1 Tokiwadai, Ube, Yamaguchi 755-8611, Japan*
[e] *Institute of Advanced Science, Yokohama National University, 79-5 Tokiwadai, Hodogaya-ku, Yokohama, Kanagawa, 240-8501, Japan*
[f] *Chemical Engineering Department, Kanagawa Institiute of Industrial Science and Technology, 705-1 Shimoimaizumi, Ebina, Kanagawa, 243-0435, Japan*

Materials

2-(2-Methoxyethoxy)ethanamine (≥95.0%) and trifluoromethanesulfonic anhydride (>98.0%) were purchased from Fluorochem Ltd. Triethylamine (>99.0%) was obtained from Tokyo Chemical Industry Co., Ltd., Tokyo, Japan. Anhydrous solvents such as dichloromethane, acetonitrile and pentane (super dehydrated grade, <10 ppm water) were supplied by FUJIFILM Wako Chemicals U.S.A. Corporation. Lithium hydride (≥95%), 1-(3-aminopropoxy)-2-methoxyethane (≥97%), hydrochloric acid solution (6 M), and sulfuric acid (>95.0%) were purchased from Sigma-Aldrich, Combi-Blocks Inc., and FUJIFILM Wako Chemicals U.S.A. Corporation, respectively. All chemicals were used as received.

Synthetic Procedures

All the reactions were conducted using Schlenk techniques.[1]

H[TfN2O2O1]: (2-(2-methoxyethoxy)ethyl)((trifluoromethyl)sulfonyl)amide

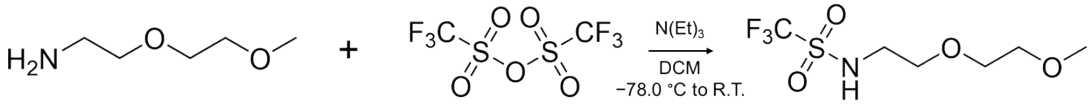

2-(2-Methoxyethoxy)ethanamine (10.12 g, 85 mmol, 1.00 equiv.) and triethylamine (18.0 mL, 13.11 g, 133 mmol, 1.52 equiv.) were stirred in 180 mL of dry dichloromethane at −78 °C in a dry ice bath under Schlenk conditions. Trifluoromethanesulfonic anhydride (15.7 mL, 26.39 g, 94 mmol, 1.10 equiv.) in 80 mL of dry dichloromethane was then added dropwise at a rate of approximately 1.5 mL/min. After the addition was complete, the reaction mixture was allowed to warm to room temperature and stirred for 5 h. Dichloromethane was removed using a rotary evaporator, yielding a colorless, transparent liquid. To the residue, 35 mL of 4 M NaOH was added, followed by three washes with 40 mL of dichloromethane each. Subsequently, 40 mL of 6 M HCl was added, and the aqueous layer was extracted three times with 40 mL of dichloromethane. The combined organic layers were dried over $MgSO_4$, and the solvent was removed under reduced pressure using a rotary evaporator. Vacuum distillation (oil bath: ~48 °C, 0.04 mbar) gave 10.5 g of a colorless, transparent liquid: 2-(2-methoxyethoxy)ethyl ((trifluoromethyl)sulfonyl)amide (**H[TfN2O2O1]**) (42.0 mmol, 49% isolated yield).

^{1}H NMR (DMSO-d_6, 500 MHz, δ in ppm): 9.46 (s, 1H, N-***H***), 3.54-3.43 (m, 6H, C***H***$_2$-O-

$C_2\boldsymbol{H}_4$-O), 3.27 (t, $^3J_{H/H}$ = 10.9 Hz, 2H, N-C$\boldsymbol{H}_2$), 3.24 (s, 3H, C$\boldsymbol{H}_3$). $^{13}C\{^1H\}$ NMR (DMSO-d_6, 126 MHz, δ in ppm): 120.15 (q, $^1J_{C/F}$ = 322.3 Hz, $\boldsymbol{C}$F3), 71.71 (s, N- $\boldsymbol{C}H_2$), 70.01 (s, N-CH_2-$\boldsymbol{C}H_2$), 69.52 (s, N-C_2H_4-O-$\boldsymbol{C}_2H_4$), 58.44 (s, N-C_2H_4- O-$\boldsymbol{C}_2H_4$), 43.71 (s, $\boldsymbol{C}H_3$). ^{19}F NMR (DMSO-d_6, 471 MHz, δ in ppm): -77.42 (s, C$\boldsymbol{F}_3$).

Li[TfN2O2O1]: Lithium(2-(2-methoxyethoxy)ethyl)((trifluoromethyl)sulfonyl)amide

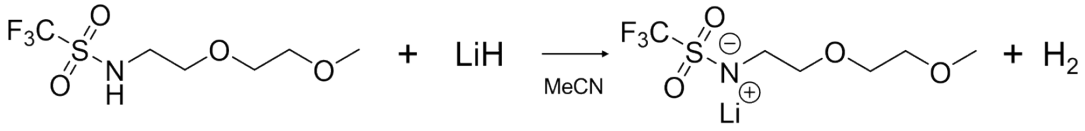

Lithium hydride (0.141 g, 18 mmol, 1.50 equiv.) was suspended in 50 mL of dry acetonitrile in a 100 mL Schlenk flask. To this suspension, 2.81 g of 2-(2-methoxyethoxy)ethyl((trifluoromethyl)sulfonyl)amide (11 mmol, 1.00 equiv.) was added slowly in an ice bath. After the addition was complete, the mixture was stirred for 1.5 h, followed by filtration through a filter cannula (glass fiber filter paper, Teflon tape, and PTFE cannula) into a separate Schlenk flask. The solvent was then removed, yielding a solid product, which was dried in vacuum at 50 °C to afford 2.54 g of lithium(2-(2-methoxyethoxy)ethyl)((trifluoromethyl)sulfonyl)amide (**Li[TfN2O2O1]**) (9.86 mmol, 88% isolated yield).

^1H NMR (DMSO-d_6, 500 MHz, δ in ppm): 3.46-3.38 (m, 4H, C$\boldsymbol{H}_2$-O-C$\boldsymbol{H}_2$), 3.27 (t, $^3J_{H/H}$ = 14.32 Hz, 2H, CH2-C$\boldsymbol{H}_2$-O), 3.22 (s, 3H, C$\boldsymbol{H}_3$), 2.97 (t, $^3J_{H/H}$ = 14.89 Hz, 2H, N-C$\boldsymbol{H}_2$). $^{13}C\{^1H\}$ NMR (DMSO-d_6, 126 MHz, δ in ppm): 123.42 (q, $^1J_{C/F}$ = 334.8 Hz, $\boldsymbol{C}F_3$), 73.54 (s, N- $\boldsymbol{C}H_2$), 71.87 (s, N-CH_2-$\boldsymbol{C}H_2$), 69.87 (s, N-C_2H_4-O-$\boldsymbol{C}_2H_4$), 58.57 (s, N-C_2H_4- O-$\boldsymbol{C}_2H_4$), 46.04 (s, $\boldsymbol{C}H_3$). ^{19}F NMR (DMSO-d_6, 471 MHz, δ in ppm): -75.69 (s, C$\boldsymbol{F}_3$). ESI-MS (negative ion mode): m/z calculated for $[TfN2O2O1]^-$ = 250.21; found = 250.14.

H[TfN3O2O1]: (3-(2-methoxyethoxy)propyl)((trifluoromethyl)sulfonyl)amide

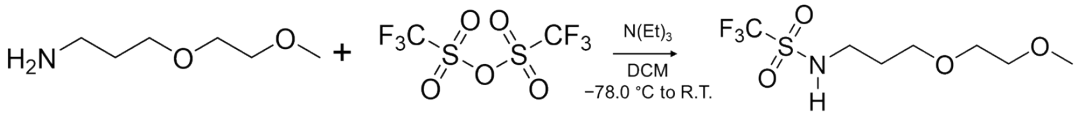

The same method used for synthesizing H[TfN2O2O1] was applied to prepare H[TfN3O2O1] . In this case, 1-(3-aminopropoxy)-2-methoxyethane (11.5 g, 86 mmol,

1.00 equiv), triethylamine (17.8 mL, 12.91 g, 128 mmol, 1.49 equiv), and trifluoromethanesulfonic anhydride (16.0 mL, 26.79 g, 94 mmol, 1.10 equiv) were used. The target product, (3-(2-methoxyethoxy)propyl)((trifluoromethyl)sulfonyl)amide (**H[TfN3O2O1]**), was obtained in 39% isolated yield.

^{1}H NMR (DMSO-d_6, 500 MHz, δ in ppm): 9.32 (s, 1H, N-***H***), 3.48-3.41 (m, 6H, C***H***$_2$-O-C$_2$***H***$_4$), 3.23 (s, 3H, C***H***$_3$), 3.19 (t, $^{3}J_{H/H}$ = 14.32 Hz, 2H, N-C***H***$_2$), 1.71 (quint, $^{3}J_{H/H}$ = 26.35 Hz, 2H, N-CH$_2$-C***H***$_2$).^{13}C{^{1}H} NMR (DMSO-d_6, 126 MHz, δ in ppm): 120.20 (q, $^{1}J_{C/F}$ = 323.4 Hz, ***C***F$_3$), 71.74 (s, N-C$_2$H$_4$-***C***H$_2$), 69.91 (s, O-CH$_2$-***C***H$_2$-O), 67.42 (s, O-***C***H$_2$-CH$_2$-O), 58.58 (s, N-***C***H$_2$), 41.27 (s, N-CH$_2$-***C***H$_2$), 30.39 (s, ***C***H$_3$).^{19}F NMR (DMSO-d_6, 471 MHz, δ in ppm): -77.30 (s, C***F***$_3$).

Li[TfN3O2O1]

: Lithium(3-(2-methoxyethoxy)propyl)((trifluoromethyl)sulfonyl)amide

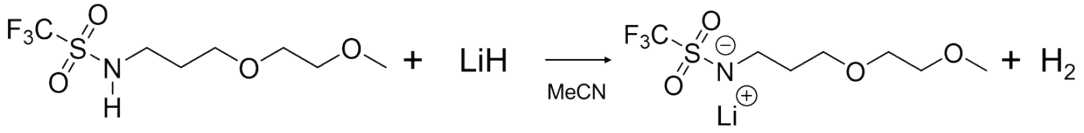

The same method used for synthesizing Li[TfN2O2O1] was applied to prepare Li[TfN3O2O1]. Lithium hydride (0.20 g, 18 mmol, 1.48 equiv.) was reacted with (3-(2-methoxyethoxy)propyl)((trifluoromethyl)sulfonyl)amide (4.5 g, 17 mmol, 1.00 equiv.). The reaction yielded 3.7 g of lithium(3-(2-methoxyethoxy)propyl)((trifluoromethyl)sulfonyl)amide (**Li[TfN3O2O1]**) (13 mmol, 80% isolated yield).

^{1}H NMR (DMSO-d_6, 500 MHz, δ in ppm): 3.43-3.35 (m, 6H, C***H***$_2$-O-C$_2$***H***$_4$), 3.22 (s, 3H, C***H***$_3$), 2.87 (t, $^{3}J_{H/H}$ = 13.17 Hz, 2H, N-C***H***$_2$), 1.50 (quint, $^{3}J_{H/H}$ = 26.92 Hz, 2H, N-CH$_2$-C***H***$_2$).^{13}C{^{1}H} NMR (DMSO-d_6, 126 MHz, δ in ppm): 123.91 (q, $^{1}J_{C/F}$ = 335.3 Hz, ***C***F$_3$), 71.83 (s, N-C$_2$H$_4$-***C***H$_2$), 69.84 (s, O-CH$_2$-***C***H$_2$-O), 69.67 (s, O-***C***H$_2$-CH$_2$-O), 58.57 (s, N-***C***H$_2$), 43.22 (s, N-CH$_2$-***C***H$_2$), 33.70 (s, ***C***H$_3$).^{19}F NMR (DMSO-d_6, 471 MHz, δ in ppm): −75.50 (s, C***F***$_3$). ESI-MS (negative ion mode): m/z calculated for [TfN3O2O1]$^{-}$ = 264.24; found = 264.17.

Thermal properties

Thermogravimetric analysis (TGA) was performed using an STA7200 and TG/DTA6200 Thermogravimetry/Differential Thermal Analyzer (Hitachi High-Tech Science Corporation). The decomposition temperature (T_d) was defined as the temperature corresponding to a 5% weight loss. During the measurement, samples were heated from 30 °C to 550 °C at a rate of 10 °C/min.

Table S1. Decomposition temperatures of the Li salts.

Li salt	T_{99} / °C	T_{95} / °C
Li[TfN2O2O1]	235.1	251.9
Li[TfN3O2O1]	141.0	257.0

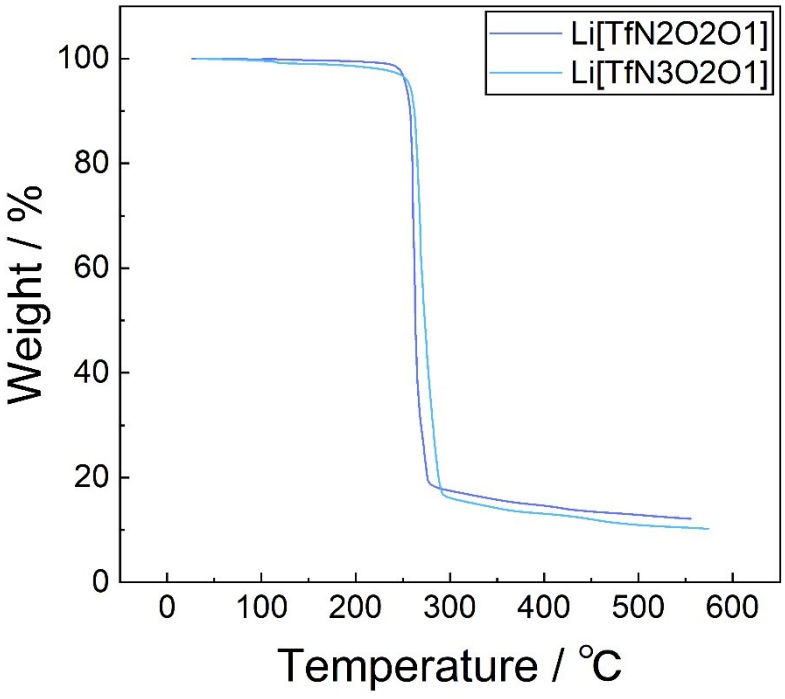

Fig. S1. TGA curves of Li[TfN2O2O1] and Li[TfN3O2O1].

Differential scanning calorimetry (DSC) measurements were performed using a Hitachi DSC7020 equipped with liquid nitrogen cooling. Samples were sealed in aluminium pans (3 MPa, diameter: 6 mm, height: 4 mm, volume: 15 μL; Hitachi) inside an Ar-filled glovebox. The pans were first heated to 80 °C, then cooled to -100 °C, and finally reheated to 200 °C at a rate of 10 °C min^{-1}. The final heating cycle was used for analysis. The melting point (T_m) was determined as the intersection between the extrapolated baseline before the endothermic event and the tangent at the inflection point of the baseline shift.

Table S2. Melting point (T_m), fusion enthalpy (ΔH_f), and fusion entropy (ΔS_f) of Li[TfN2O2O1], Li[TfN3O2O1], and Li[FTA] derived from DSC curves.

	T_m / °C	ΔH_f / kJ mol^{-1}	ΔS_f / J mol^{-1} K^{-1}
Li[TfN2O2O1]	95.5	17.5	47.0
Li[TfN3O2O1]	108.3	27.4	70.6
Li[FTA]	97.0	17.5	46.8

Crystallography

Crystals were obtained using the vapor diffusion method. The solvents used were dichloromethane and acetonitrile for Li[TfN2O2O1], and dichloromethane and pentane for Li[TfN3O2O1]. X-ray diffraction data were collected on a Rigaku XtaLAB AFC12 Kappa diffractometer with dual offset geometry using Cu Kα radiation (λ = 1.54184 Å). Data reduction and structure refinement were carried out using CrysAlisPro and Olex2, respectively. Crystallographic data have been deposited with the CCDC numbers 2473175 (**Li[TfN3O2O1]**) and 2473176 (**Li[TfN2O2O1**]), and are summarized below in CIF format.

Table S3. Summary of crystal structures.

	Li[TfN2O2O1]	Li[TfN3O2O1]
Empirical formula	$C_6H_{11}F_3LiNO_4S$	$C_{14}H_{26}F_6Li_2N_2O_8S_2$
Formula weight (g / mol)	257.16	542.37
Crystal system	monoclinic	Monoclinic
Space group	$P2_1/c$	$P2_1/n$
a (Å)	9.18030(10)	7.29450(10)
b (Å)	20.92980(10)	8.96000(10)
c (Å)	18.25210(10)	18.6185(2)
α (°)	90	90
β (°)	97.4210(10)	95.3830(10)
γ (°)	90	90
Volume (Å^3)	3477.62(5)	1211.51(3)
Z	12	2
Density (calc.) (g/cm^3)	1.473	1.487
Absorption coefficient		
F(000)	1584.0	560.0
2θ range (°)	12.872~133.188	12.668~133.186
Reflections collected	40088	11780
Independent reflections	6097	2152
Data / restraints / parameters	6097/6/447	2152/0/156
Goodness-of-fit on F^2	1.0250	1.105
Final R indices [I>2σ(I)]	R_1 = 0.0407 wR_2 = 0.1072	R_1 = 0.0651 wR_2 = 0.1675
R indices (all data)	R_1 = 0.0428 wR_2 = 0.1090	R_1 = 0.0670 wR_2 = 0.1702
Largest diff. peak/hole (eÅ^{-3})	0.63/−0.32	0.99/−0.48

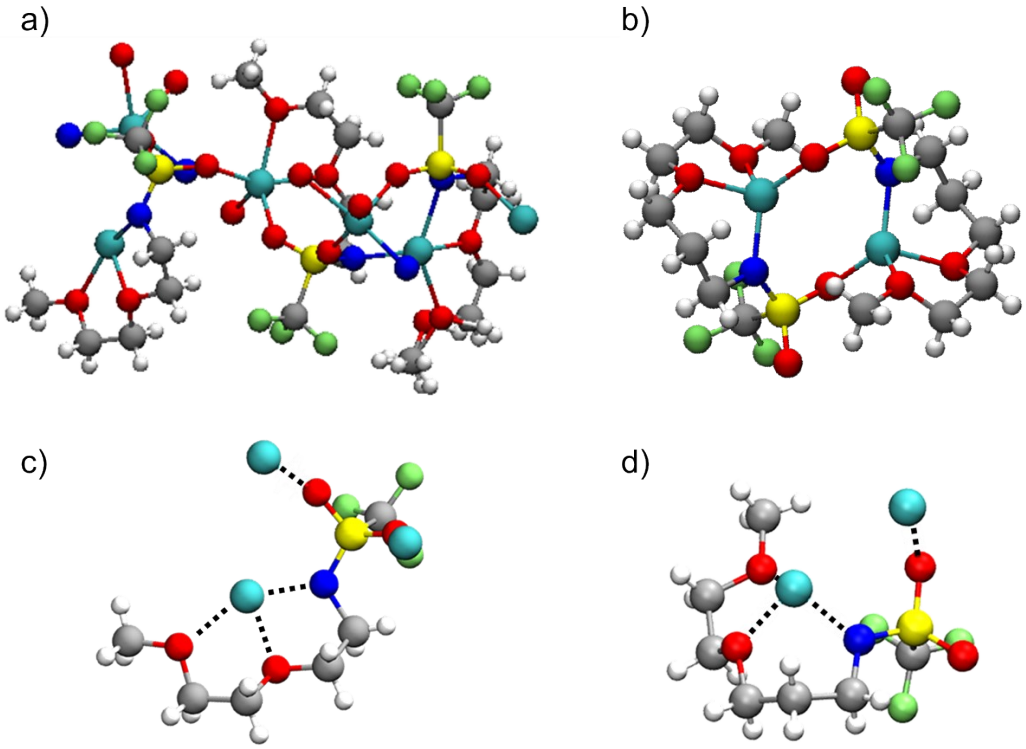

Fig. S2 Crystal structure image of Li[TfN2O2O1] and Li[TfN3O2O1]: (a,b) aggregate structure that incorporates Li ions (Li[TfN2O2O1] and Li[TfN3O2O1], respectively); (c,d) part of the coordination structure (Li[TfN2O2O1] and Li[TfN3O2O1] respectively).

The Li ion in Li[TfN3O2O1] is four-coordinate in a slightly distorted tetrahedral geometry. In contrast, Li[TfN2O2O1] contains three crystallographically distinct Li ions with different coordination environments: Li1 has an N_2O_3 donor set, whereas Li2 and Li3 both have N_1O_4 donor sets. Examination of the τ_5 parameters for each Li ion show that Li1 (0.30) and Li2 (0.29) are both severely distorted away from ideal square-based pyramidal geometry, whereas Li3 (0.07) is much closer to ideal square-based pyramidal. The Li–N distances in Li[TfN2O2O1] are in a range from 2.061(4)–2.345(5) Å, all much longer than the Li–N distance in Li[TfN3O2O1] of 1.989(4) Å. Similarly, the average Li–O bond length in Li[TfN2O2O1] of 2.082 Å is longer than the average Li–O bond length in Li[TfN3O2O1] of 1.964 Å. These data suggest that the extra methylene group in the [TfN3O2O1] anion imparts additional flexibility to the anion which enables it to occupy more of the coordination sphere of the small Li ion, compared to the slightly smaller and less flexible [TfN2O2O1] anion. This is why Li[TfN2O2O1] forms a coordination polymer in the solid state with weaker anion-cation interactions, likely resulting in its reduced ΔH_f compared to the dimeric Li[TfN3O2O1] with its stronger anion-cation interactions.

Raman spectroscopy

Raman spectra of the solid and molten states of the Li salts were recorded using a laser Raman spectrometer (NRS-4100, JASCO Co., Ltd.) equipped with a 785 nm laser. Samples were sealed in glass capillaries (1 mm inner diameter) inside an Ar-filled glovebox. The instrument was calibrated using a polypropylene standard. For measurements in the molten state, the sample was first heated to 100 °C in an oil bath to induce melting and subsequently measured at ambient temperature in the supercooled state.

Quantum chemical calculations

Ab initio and DFT calculations were performed using Gaussian 16.[2] Basis set superposition error (BSSE)[3] was corrected for all intermolecular interaction energy (E_{int}) calculations using the counterpoise method.[4] The stabilization energy due to complex formation from isolated species (E_{form}) was calculated as the sum of E_{int} and deformation energy (E_{def}), which is the increase in energy of the anion due to the deformation of geometry associated with complex formation.[5] Torsional angle was fixed and other internal geometrical parameters were optimized in the calculations of torsional potentials. The optimized geometries of isolated molecules at the MP2/6-311G** level were used for the calculations of intermolecular interaction energy potentials without further geometry optimizations.

MD simulation

MPDynPFF software was used with a polarizable force field for MD simulations.[6, 7] MD simulations were carried out using the *NPT* ensemble. All C-H bonds were fixed using the SHAKE/RATTLE algorithm.[8] Reversible RESPA was used for multiple-time-step integration of the atomic motions.[8, 9] The time step of 8 fs was used for updating interactions in the Ewald reciprocal space, and 2 fs was used for other interactions. A periodic boundary condition was employed. Nonbonded forces were truncated at 12 Å, and the Coulomb interactions were computed using the Ewald method.[10] Constant temperature and pressure (0.1 MPa) were maintained using the Nosé–Hoover chain thermostat[11] and Andersen barostat.[12] The time constants for the thermostat and barostat were 0.5 and 2.0 ps, respectively. The polarizable force field[13] was designed to reproduce intermolecular interaction energies between Li^+ and the oxygen or nitrogen atoms of the anion, which is essential to reproduce coordination structures in classical MD simulations. Details of the polarizable force field are shown in **Table S4** and **Figs. S3** and **S4**.

To minimize possible artifacts in the initial configurations, the system was equilibrated at 230 °C, starting from a low-density condition 1 ns prior to equilibration at the production run temperature (100, 120 and 140 °C, respectively). The density, radial distribution functions and cumulative coordination numbers were evaluated from the 4 ns of MD trajectories after the equilibration run. The self-diffusion coefficients of the ions were calculated from mean square displacements obtained from the 30 ns of MD trajectories after equilibration. Herein, 120 ion pairs were used in the simulations.

Fig. S5 shows snapshots of molten Li[TfN2O2O1]. The anionic moieties (SO_2N groups) of $[TfN2O2O1]^-$ and Li ions form complexes (**Fig. S5a**). Meanwhile, some oxygen atoms in the ether chains are not coordinated with Li ions (**Fig. S5b**). The complex formed in the molten state, consisting of $Li_3[TfN2O2O1]_3$ is shown in **Fig. S5c**. This complex exhibits a micelle-like structure. The polar moieties (SO_2N groups) of $[TfN2O2O1]^-$ and Li ions form aggregates, surrounded by less polar ether chains.

Table S4. Force field parameters used for MD simulations (Atom types were explained in Figure S3).

Nonbonding parameters

atom	σ (Å)	ε (kcal mol^{-1})	α (a.u.)
NIE	3.55	0.17	7.4
SO	3.55	0.25	16.0
OS	3.00	0.13	5.0
CF	3.50	0.066	9.0
FC	3.15	0.053	5.3
CS	3.50	0.066	9.0
CT	3.50	0.066	9.0
OG	3.10	0.140	4.0
HC	2.50	0.030	2.0
Li	2.48	0.003	0.0

$$E_{\text{nonbond}} = 4\varepsilon[(\sigma/r)^{12} - \sigma(\sigma/r)^{6}]$$

Bond stretching parameters

bond	k_s (kcal mol^{-1} Å^{-2})	r_0 (Å)
NIE-SO	744.0	1.546
SO-OS	1274.0	1.450
SO-CF	471.0	1.835
CF-FC	884.0	1.340

NIE-CS	268.0	1.454
CS-CS	268.0	1.529
OG-CS	570.0	1.408
OG-CT	570.0	1.408
CS-HC	340.0	1.090
CT-HC	340.0	1.090

$E_{str} = k_s (r - r_0)^2$

Angle bending parameters

angle	k_θ (kcal mol^{-1} rad^{-2})	θ_0 (deg)
SO-NIE-CS	80.00	112.0
NIE-SO-OS	189.00	118.0
NIE-SO-CF	195.00	105.2
OS-SO-OS	232.00	120.2
OS-SO-CF	208.00	102.6
SO-CF-FC	166.00	110.4
CS-CS-HC	37.50	110.7
NIE-CS-CS	58.35	107.7
NIE-CS-HC	37.50	110.7
HC-CS-HC	33.00	107.8
CS-CS-OG	80.00	109.0
OG-CS-HC	35.00	109.0
CS-OG-CS	55.00	106.8
CS-OG-CT	55.00	106.8
OG-CT-HC	35.00	109.0
HC-CT-HC	33.00	107.8

$E_{bend} = k_\theta (\theta - \theta_0)^2$

Torsional parameters

dihedral	V_1 (kcal mol^{-1})	V_2 (kcal mol^{-1})	V_3 (kcal mol^{-1})
FC-CF-SO-NIE	0.0	0.0	0.300
FC-CF-SO-OS	0.0	0.0	0.171
CS-NIE-SO-CF	-4.000	3.700	0.0
CS-NIE-SO-OS	0.0	0.0	0.0
SO-NIE-CS-CS	-8.000	-1.500	0.0
SO-NIE-CS-HC	0.0	0.0	0.0
OG-CS-CS-NIE	4.300	4.000	0.202
NIE-CS-CS-HC	0.0	0.0	0.0
OG-CS-CS-HC	0.0	0.0	0.0
HC-CS-CS-HC	0.0	0.0	3.180
CS-CS-OG-CS	-0.980	-0.970	0.250
OG-CS-CS-OG	4.300	4.000	0.202
CS-CS-OG-CT	-1.900	-0.970	0.250
HC-CS-OG-CS	0.0	0.0	0.670
HC-CS-OG-CT	0.0	0.0	0.670
HC-CT-OG-CS	0.0	0.0	0.670

$E_{\text{torsion}} = \Sigma\ V_n/2\ (1 + \cos(n\phi))$

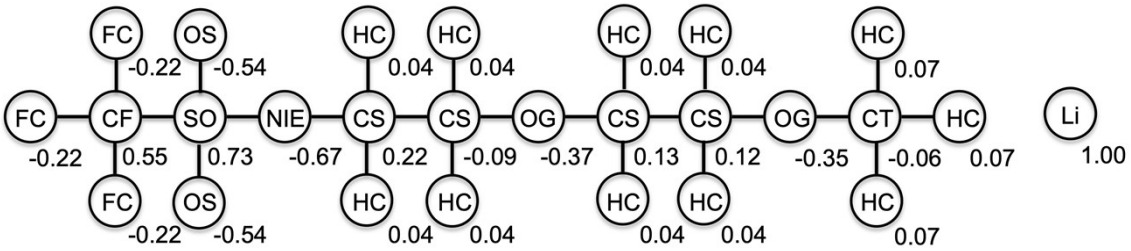

Fig. S3 Atom types and atomic charges used for MD simulations.

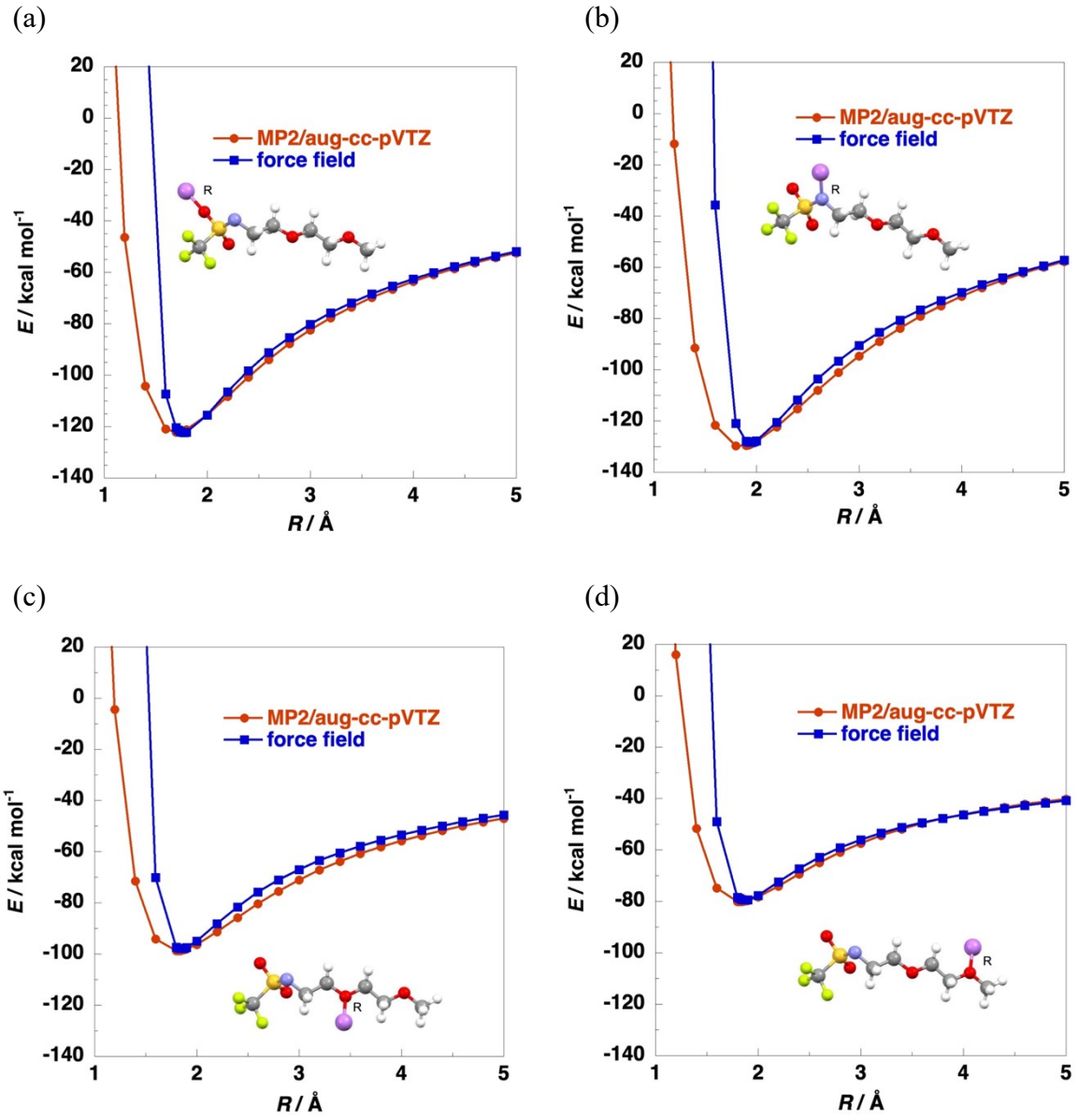

Fig. S4 Intermolecular interaction energy potentials calculated for Li[TfN2O2O1] complex at MP2/aug-cc-pVTZ level with changing Li…O or Li…N distances (*R*); (a) Li^+ is located on the extension of the S-O bond; (b) Li^+ is located on the bisector of the S-N-C angle; (c, d) Li^+ is located on the bisector of the C-O-C angle.

(a) (b) (c)

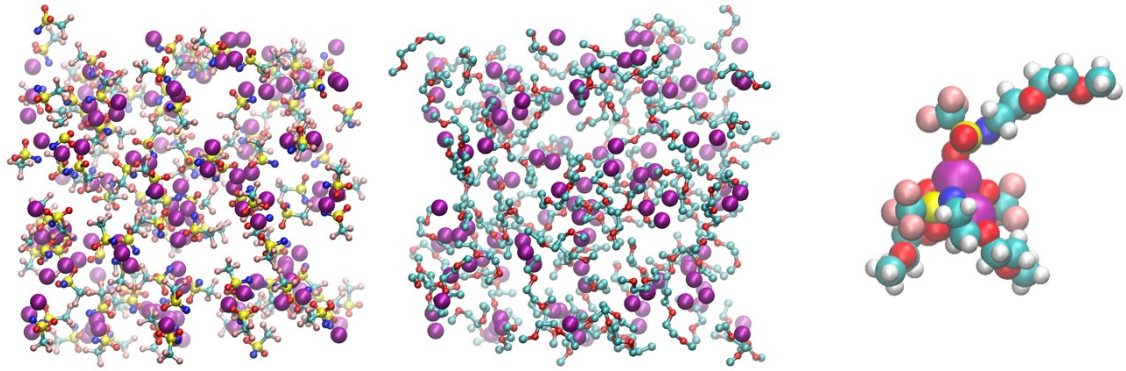

Fig. S5 Snapshots of Li[TfN2O2O1] in the molten state at 413.15 K with 120 ion pairs. Colors of carbon, oxygen, nitrogen, fluorine, sulfur and lithium are light blue, red, blue, pink, yellow and violet; (a) Li ions and anionic TfN moieties, (b) Li ions and ether chains, (c) a Li3[TfN2O2O1]3 complex formed in the molten state.

Lithium Transference Number

Li ion transference number under anion blocking condition (t_{Li^+}) was obtained by the potentiostatic polarization combined with the electrochemical impedance spectroscopy (EIS) using Li/Li symmetric 2032 coin-type cells.[14-16] Two circular pieces punched out of Li foil (Honjo Metal Co., Ltd.) of 16 mm diameter and 0.2 mm thickness were used as the electrodes. The measurements were performed using ModuLab XM ECS (Solartron Analytical). The interfacial impedance was confirmed to be unchanged prior to the t_{Li^+} measurements via the EIS measurements. After that, the further EIS measurements were performed before/after potentiostatic polarization at 5 mV in a frequency range from 1 MHz to 0.1 Hz with an amplitude of 5 mV (Fig. S4). t_{Li^+} was calculated by the following equation,

$$t_{Li}^{+} = \frac{I_{ss}(\Delta V - I_{ohm}R_0)}{I_{ohm}(\Delta V - I_{ss}R_{ss})}$$

where I_{ohm} is the initial current, I_{ss} is the steady-state current obtained during potentiostatic polarization. R_0 and R_{ss} are the initial and steady-state interfacial resistances obtained by EIS, respectively. ΔV is the applied voltage. I_{ohm} is calculated from Ohm's law, $I_{ohm} = {\Delta V}/{(R_{bulk} + R_0)}$, where R_{bulk} is the resistance of the bulk electrolyte.

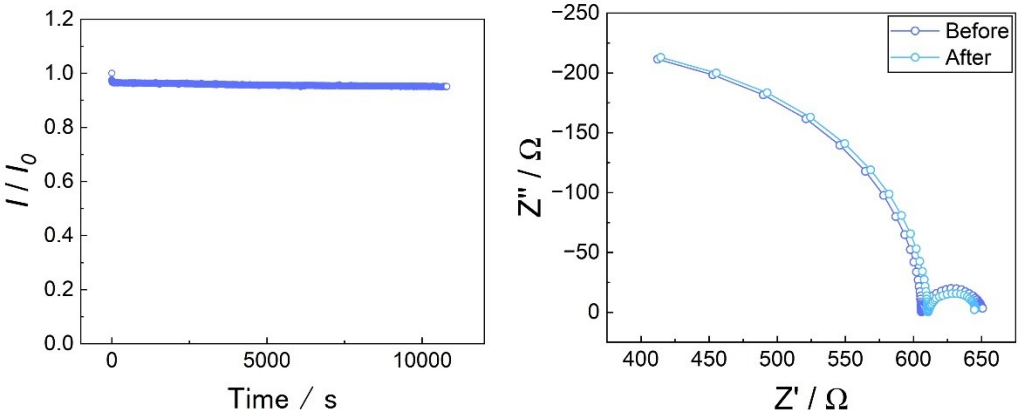

Fig. S6 The potentiostatic polarization curves and Nyquist plots before and after the potentiostatic polarization of Li/Li symmetric cells using Li[TfN2O2O1] at 120 °C.

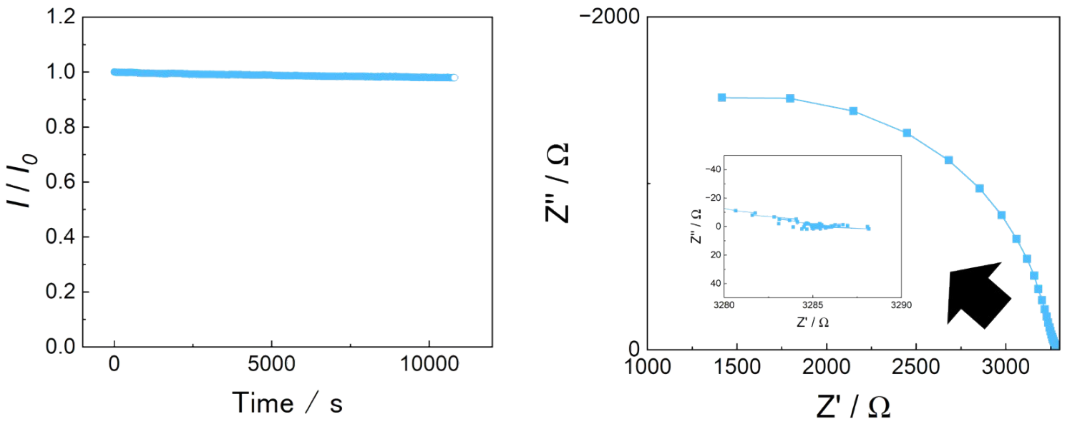

Fig. S7 The potentiostatic polarization curves and Nyquist plots of Li/Li symmetric cells using Li[TfN3O2O1] at 130 °C.

Ionic conductivity

Ionic conductivity was measured by the complex impedance method using a VMP3 (Biologic Science Instruments Ltd.) in the frequency range of 500 kHz–1 Hz with a voltage amplitude of 10 mV. The cell constants of screw-type conductivity cells equipped with SUS electrodes (MIC LAB Co., Ltd.) were determined prior to measurement using a 0.01 mol dm^{-3} KCl aqueous solution at 25 °C. The experimental uncertainty in conductivity values was determined to be within ±12% across the measured temperature range.

Table S5. Ionic conductivity of the Li salts measured in the temperature range from 140 °C to 60 °C.

	T / °C	σ / S cm^{-1}	logσ
Li[TfN3O2O1]	120	6.35×10^{-6}	−5.20
	110	3.63×10^{-6}	−5.44
	100	1.91×10^{-6}	−5.71
	90	9.18×10^{-7}	−6.04
	80	3.94×10^{-7}	−6.40
	70	1.80×10^{-7}	−6.74
Li[TfN2O2O1]	130	2.73×10^{-5}	−4.56
	120	1.77×10^{-5}	−4.75
	110	9.06×10^{-6}	−5.04
	100	4.83×10^{-6}	−5.32
	90	2.27×10^{-6}	−5.64
	80	9.50×10^{-7}	−6.02
	70	3.35×10^{-7}	−6.47
	60	9.65×10^{-8}	−7.02
Li[FTA]	140	4.74×10^{-5}	−4.32
	130	2.14×10^{-5}	−4.67
	120	9.54×10^{-6}	−5.02
	110	4.78×10^{-6}	−5.32
	100	2.27×10^{-6}	−5.64

Diffusivity

Pulsed-field gradient nuclear magnetic resonance (PFG-NMR) measurements were conducted using a JEOL ECX-400 spectrometer equipped with a 9.4 T narrow-bore superconducting magnet, a JEOL pulsed-field gradient probe, and a current amplifier. The self-diffusion coefficients of Li ions and anions were measured as follows: anions (^{19}F, 376.1 MHz), and Li ions (^{7}Li, 155.3 MHz). Samples were prepared in NMR microtubes (BMS-005J, Shigemi, Tokyo, Japan) with a sample height of less than 5 mm to suppress convective flow. The experimental procedure for PFG-NMR measurements has been described in detail elsewhere.[17, 1814,15]

Table S6. Self-diffusion coefficients of the lithium salts in their molten state, as determined by PFG-NMR.

sample	ion	Temp. / °C	D / 10^{-7} cm^2 s^{-1}	Log(D)
Li[TfN2O2O1]	Li^+	120	0.103	−0.986
		140	0.280	−0.553
	$[TfN2O2O1]^-$	120	0.106	−0.974
		140	0.274	−0.562
Li[TfN3O2O1]	Li^+	140	0.353	−0.452
	$[TfN3O2O1]^-$	140	0.387	−0.412
Li[FTA]	Li^+	100	0.0242	−1.62
		120	0.0620	−1.21
		140	0.151	−0.821
	$[FTA]^-$	120	0.0289	−1.54
		140	0.0745	−1.13

Electrochemical properties

Cyclic voltammetry (CV) and linear sweep voltammetry (LSV) were carried out using a 2032-type stainless-steel coin cell holder at 120 °C for Li[TfN2O2O1] and 130 °C for Li Li[TfN3O2O1]. The electrochemical window was evaluated using a copper working electrode in the negative potential region (−0.1 to +1.5 V vs. Li/Li^+) and a stainless-steel (SUS) working electrode in the positive potential region (+2.0 to +5.5 V vs. Li/Li^+).

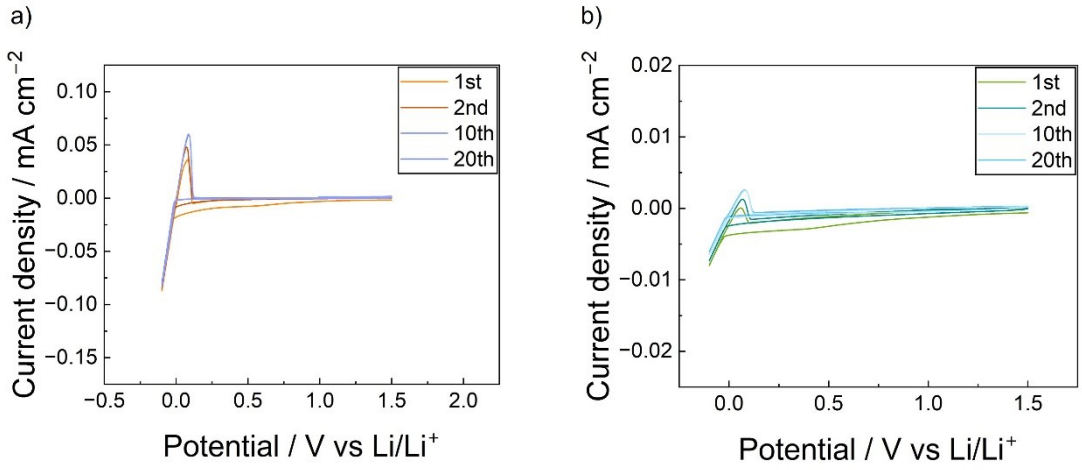

Fig. S8 Cyclic voltammograms on Cu electrode at scan rate 1 mV s^{-1}; a) Li[TfN2O2O1] at 120 ℃ and b) Li[TfN3O2O1] at 130 ℃.

NMR and MS Spectra

H[TfN2O2O1]

^{1}H NMR

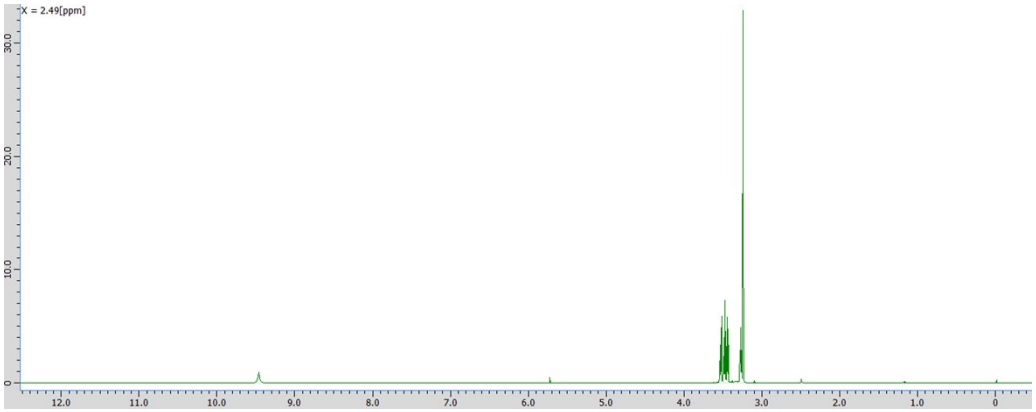

^{13}C NMR

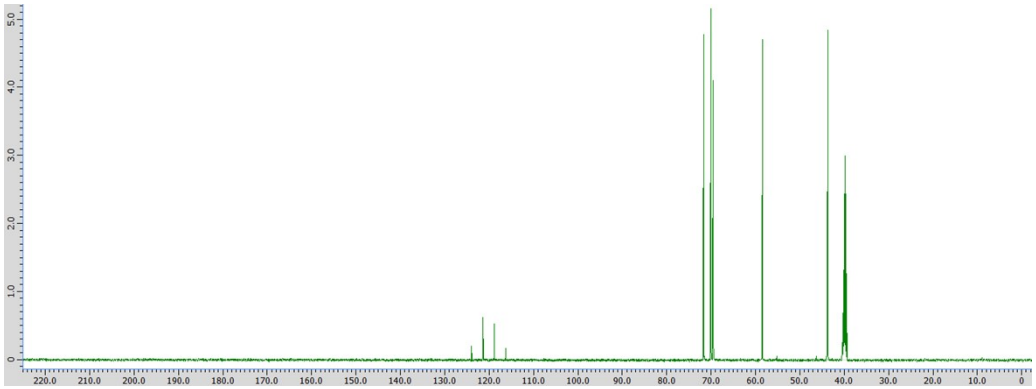

^{19}F NMR

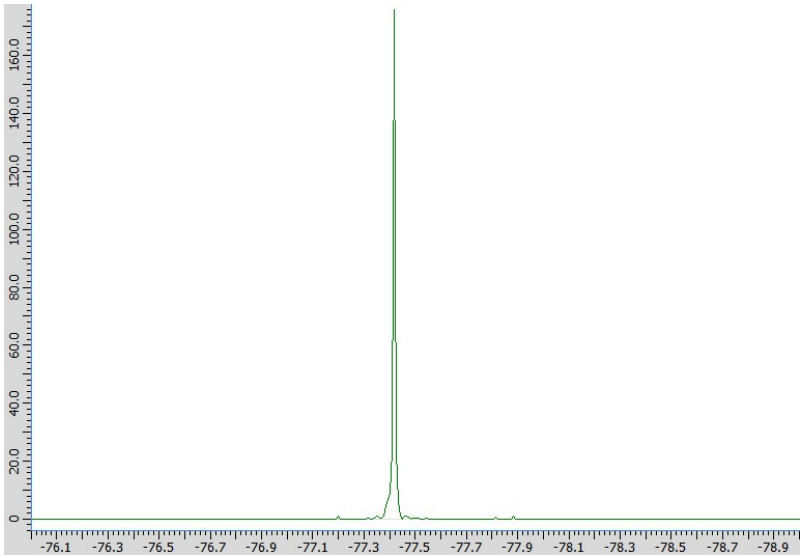

Li[TfN2O2O1]

^{1}H NMR

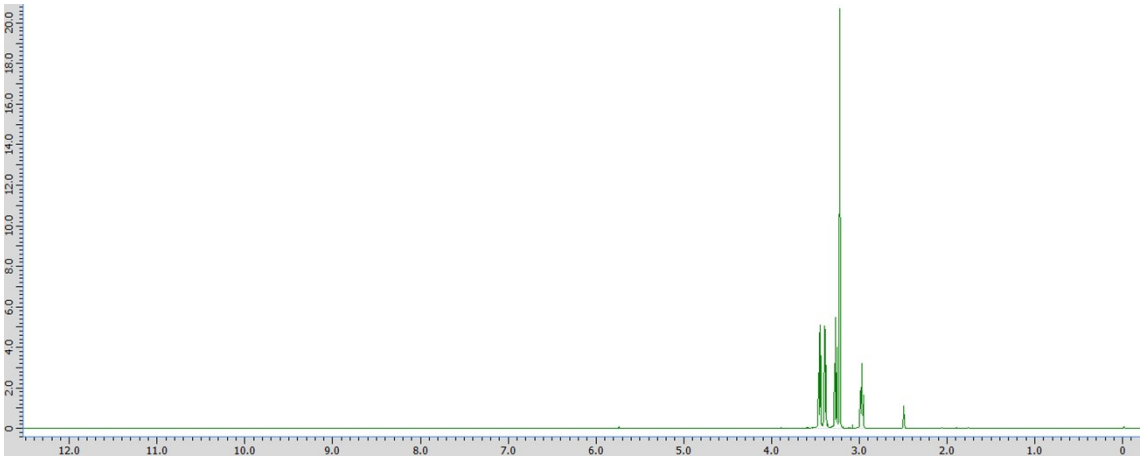

^{13}C NMR

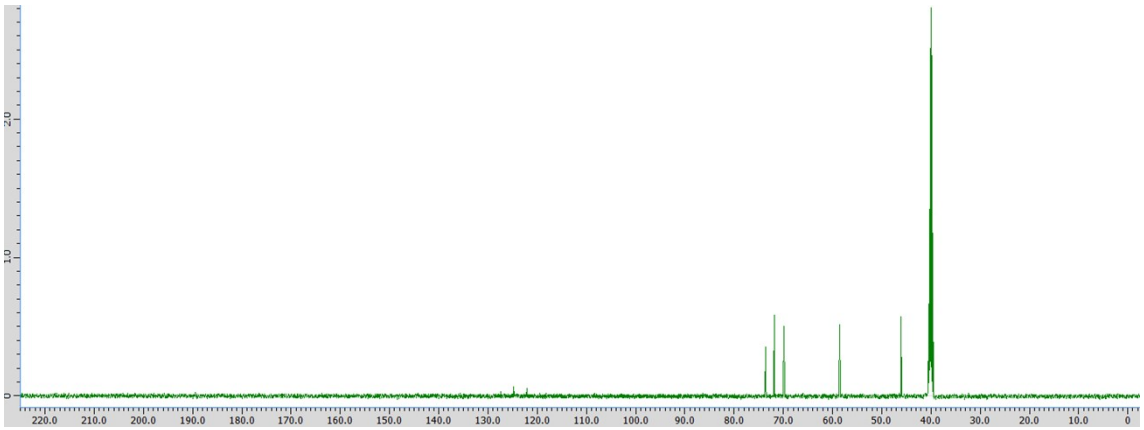

^{19}F NMR

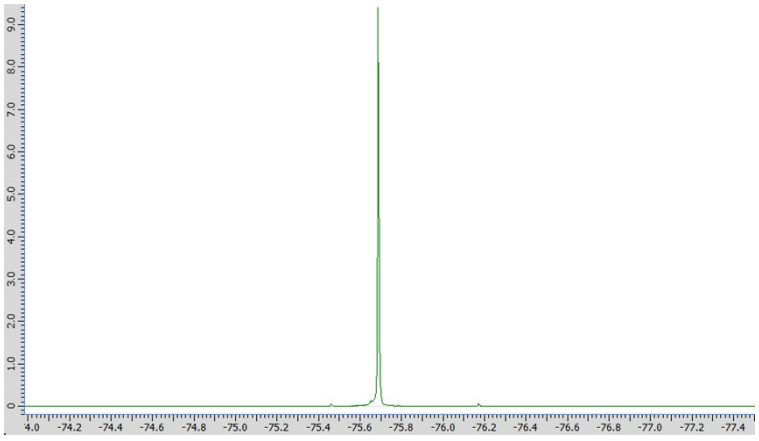

EIS-MS

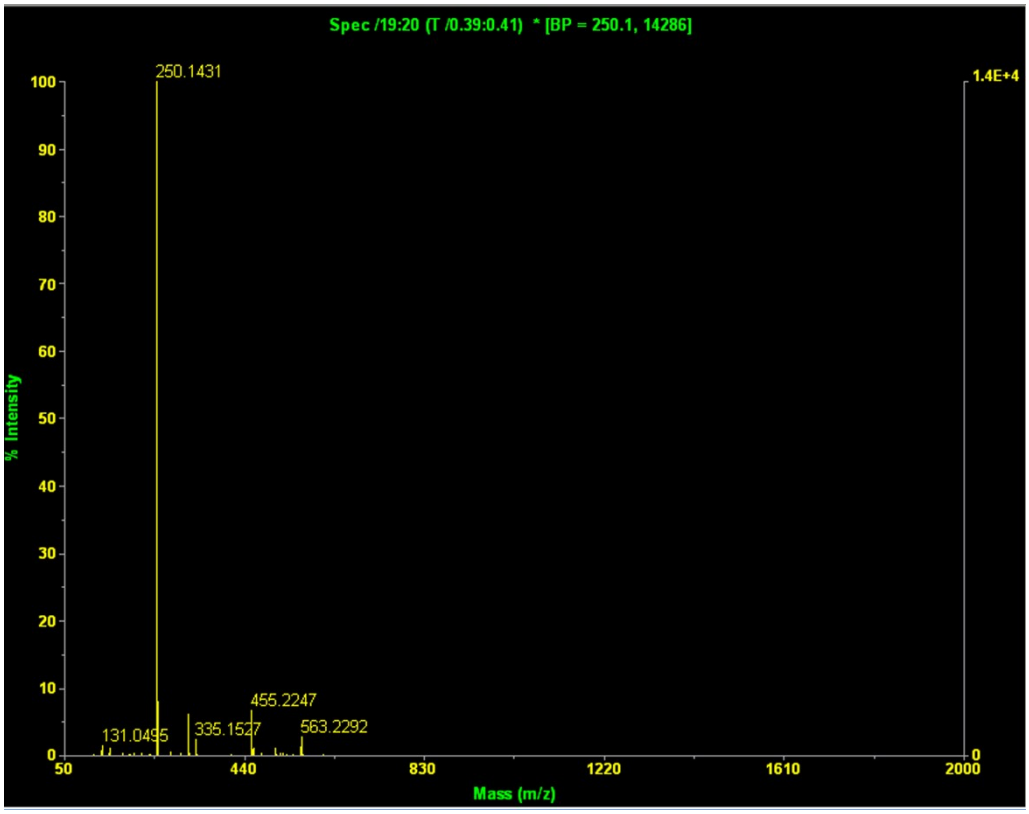
Spec /19:20 (T /0.39:0.41) * [BP = 250.1, 14286]
250.1431
1.4E+4
100
90
80
70
60
50
40
30
20
10
0
% Intensity
455.2247
131.0495
335.1527
563.2292
0
50
440
830
1220
1610
2000
Mass (m/z)

H[TfN3O2O1]

^{1}H NMR

^{13}C NMR

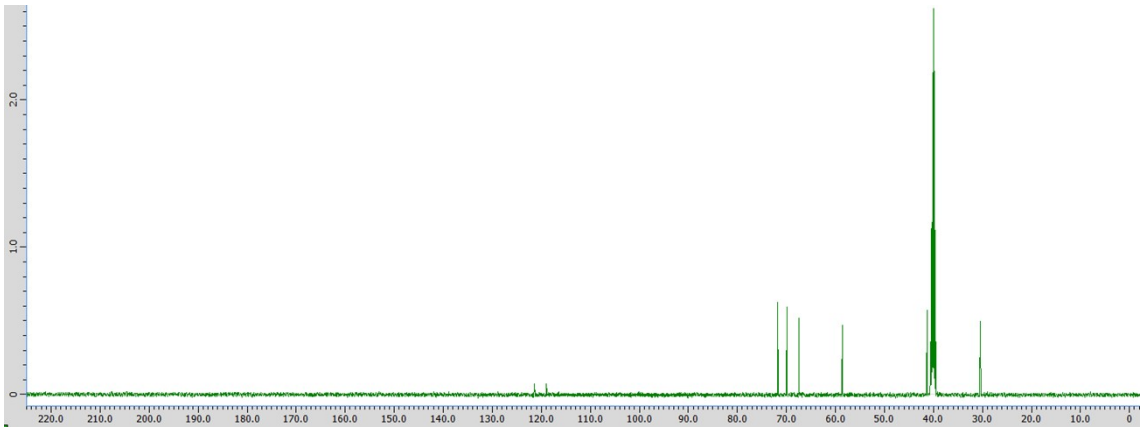

^{19}F NMR

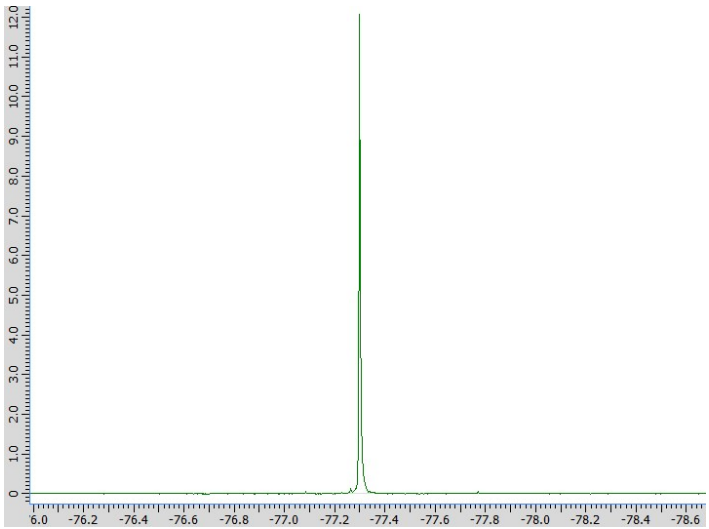

Li[TfN3O2O1]

^{1}H NMR

^{13}C NMR

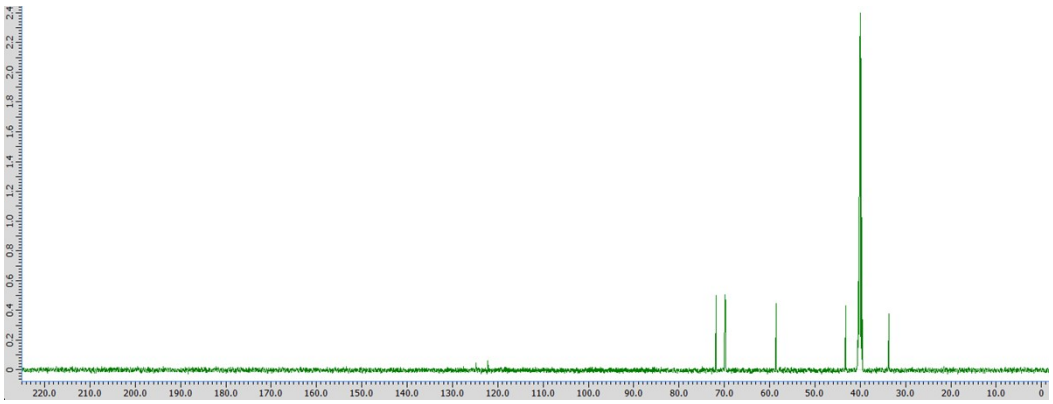

^{19}F NMR

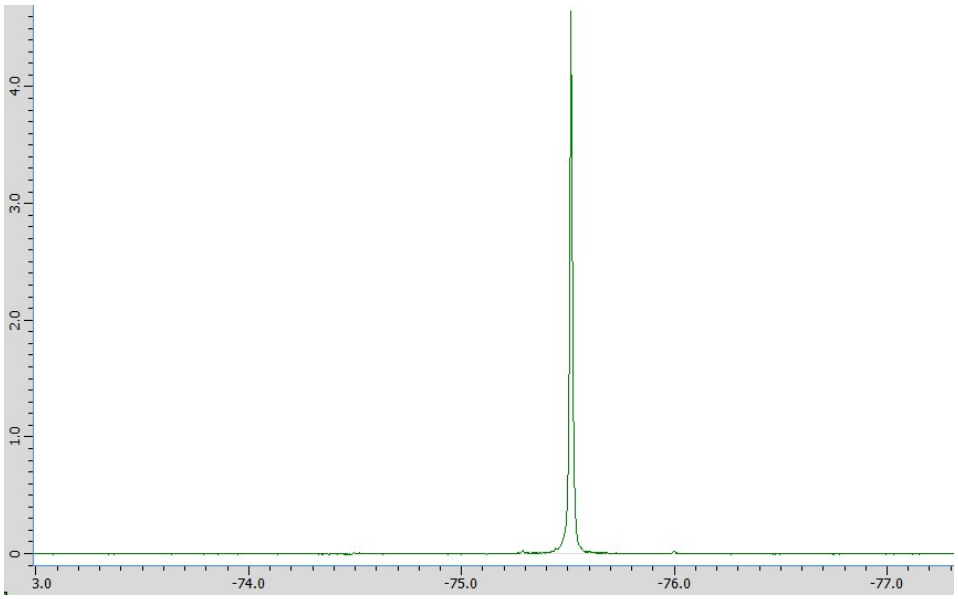

EIS-MS

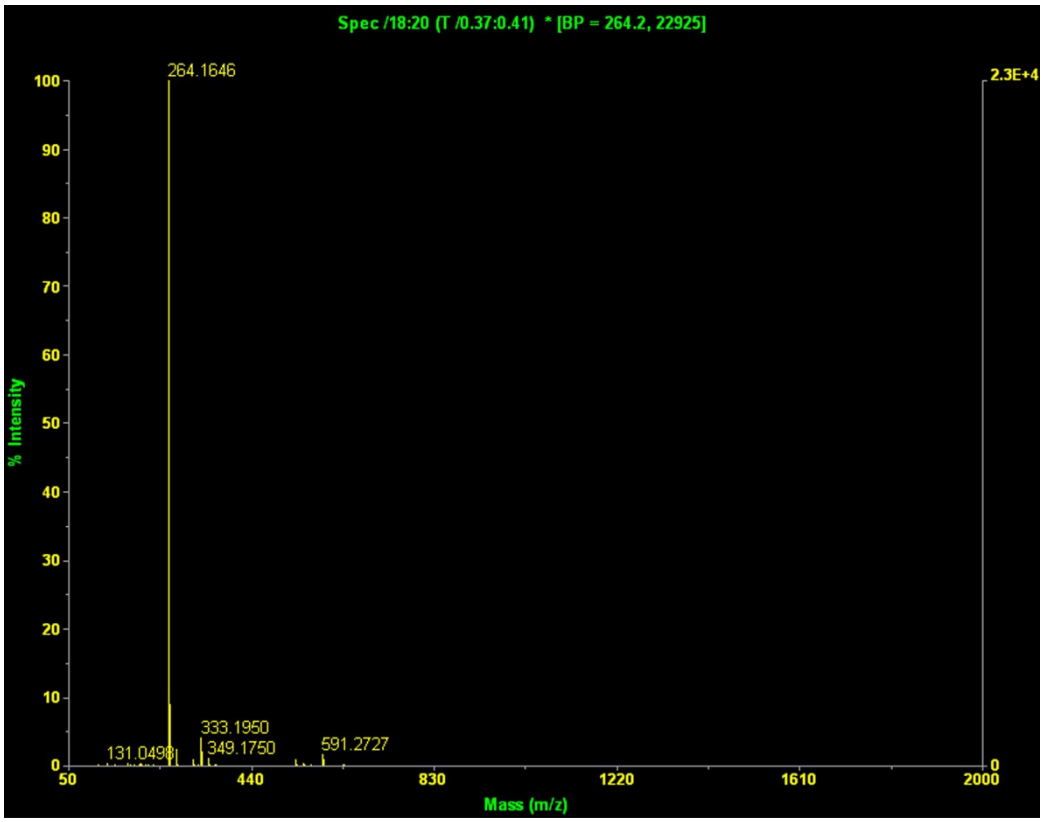

References

1. A. M. Borys, *Organometallics*, 2023, **42**, 182-196.
2. M. J. Frisch, G. W. Trucks, H. B. Schlegel, G. E. Scuseria, M. A. Robb, J. R. Cheeseman, G. Scalmani, V. Barone, G. A. Petersson, H. Nakatsuji, X. Li, M. Caricato, A. V. Marenich, J. Bloino, B. G. Janesko, R. Gomperts, B. Mennucci, H. P. Hratchian, J. V. Ortiz, A. F. Izmaylov, J. L. Sonnenberg, Williams, F. Ding, F. Lipparini, F. Egidi, J. Goings, B. Peng, A. Petrone, T. Henderson, D. Ranasinghe, V. G. Zakrzewski, J. Gao, N. Rega, G. Zheng, W. Liang, M. Hada, M. Ehara, K. Toyota, R. Fukuda, J. Hasegawa, M. Ishida, T. Nakajima, Y. Honda, O. Kitao, H. Nakai, T. Vreven, K. Throssell, J. A. Montgomery Jr., J. E. Peralta, F. Ogliaro, M. J. Bearpark, J. J. Heyd, E. N. Brothers, K. N. Kudin, V. N. Staroverov, T. A. Keith, R. Kobayashi, J. Normand, K. Raghavachari, A. P. Rendell, J. C. Burant, S. S. Iyengar, J. Tomasi, M. Cossi, J. M. Millam, M. Klene, C. Adamo, R. Cammi, J. W. Ochterski, R. L. Martin, K. Morokuma, O. Farkas, J. B. Foresman and D. J. Fox, *Journal*, 2016.
3. B. J. Ransil, *The Journal of Chemical Physics*, 1961, **34**, 2109-2118.
4. S. F. Boys and F. Bernardi, *Molecular Physics*, 1970, **19**, 553-566.
5. S. Tsuzuki, K. Hayamizu, S. Seki, Y. Ohno, Y. Kobayashi and H. Miyashiro, *The Journal of Physical Chemistry B*, 2008, **112**, 9914-9920.
6. W. Shinoda, 2022, **http://theocomp.chem.okayama-u.ac.jp/member/wshinoda/MPDyn2/**
7. W. Shinoda and M. Mikami, *Journal of Computational Chemistry*, 2003, **24**, 920-930.
8. M. Tuckerman, B. J. Berne and G. J. Martyna, *The Journal of Chemical Physics*, 1992, **97**, 1990-2001.
9. G. J. Martyna, M. E. Tuckerman, D. J. Tobias and M. L. Klein, *Molecular Physics*, 1996, **87**, 1117-1157.
10. M. P. Allen and D. J. Tildesley, *Journal*, 1987.
11. G. J. Martyna, M. L. Klein and M. Tuckerman, *The Journal of Chemical Physics*, 1992, **97**, 2635-2643.
12. H. C. Andersen, *The Journal of Chemical Physics*, 1980, **72**, 2384-2393.
13. S. Tsuzuki, S. Ikeda, W. Shinoda, K. Shigenobu, K. Ueno, K. Dokko and M. Watanabe, *The Journal of Physical Chemistry B*, 2023, **127**, 6333-6341.
14. P. G. Bruce, J. Evans and C. A. Vincent, *Solid State Ionics*, 1988, **28-30**, 918-922.
15. M. Watanabe, S. Nagano, K. Sanui and N. Ogata, *Solid State Ionics*, 1988, **28-30**, 911-917.
16. M. D. Galluzzo, J. A. Maslyn, D. B. Shah and N. P. Balsara, *The Journal of Chemical Physics*, 2019, **151**, 020901.
17. H. Tokuda, K. Hayamizu, K. Ishii, M. A. B. H. Susan and M. Watanabe, *The Journal of Physical Chemistry B*, 2005, **109**, 6103-6110.
18. T. Sudoh, K. Shigenobu, K. Dokko, M. Watanabe and K. Ueno, *Physical Chemistry Chemical*

Physics, 2022, **24**, 14269-14276.